THE JOURNAL OF BIOLOGICAL CHEMISTRY VOL. 285, NO. 6, pp. 4099–4109, February 5, 2010

Defining the Pathogenesis of the Human Atp12p W94R Mutation Using a *Saccharomyces cerevisiae* Yeast Model*

Received for publication, July 20, 2009, and in revised form, November 8, 2009 Published, JBC Papers in Press, November 20, 2009, DOI 10.1074/jbc.M109.046920

Ann Meulemans[‡1], Sara Seneca[‡1], Thomas Pribyl[§], Joel Smet[¶], Valerie Alderweirldt[‡], Anouk Waeytens[‖], Willy Lissens[‡], Rudy Van Coster[¶], Linda De Meirleir[**], Jean-Paul di Rago[‡‡], Domenico L. Gatti[§], and Sharon H. Ackerman[§2]

From the [‡]Center for Genetics and [**]Department of Pediatric Neurology, UZ Brussel, Vrije Universiteit Brussel, Brussels B-1050, Belgium, the [§]Department of Biochemistry and Molecular Biology, Wayne State University School of Medicine, Detroit, Michigan 48201, the Departments of [¶]Pediatrics and [‖]Pathology, Division of Pediatric Neurology and Metabolism, Ghent University Hospital, Ghent 9000, Belgium, and the [‡‡]Institut de Biochimie et Génétique Cellulaires CNRS/Bordeaux 2 University, Bordeaux Cedex 33077, France

Studies in yeast have shown that a deficiency in Atp12p prevents assembly of the extrinsic domain (F_1) of complex V and renders cells unable to make ATP through oxidative phosphorylation. De Meirleir *et al.* (De Meirleir, L., Seneca, S., Lissens, W., De Clercq, I., Eyskens, F., Gerlo, E., Smet, J., and Van Coster, R. (2004) *J. Med. Genet.* 41, 120–124) have reported that a homozygous missense mutation in the gene for human Atp12p (HuAtp12p), which replaces Trp-94 with Arg, was linked to the death of a 14-month-old patient. We have investigated the impact of the pathogenic W94R mutation on Atp12p structure/function. Plasmid-borne wild type human Atp12p rescues the respiratory defect of a yeast *ATP12* deletion mutant (Δatp12). The W94R mutation alters the protein at the most highly conserved position in the Pfam sequence and renders HuAtp12p insoluble in the background of Δatp12. In contrast, the yeast protein harboring the corresponding mutation, ScAtp12p(W103R), is soluble in the background of Δatp12 but not in the background of Δatp12Δfmc1, a strain that also lacks Fmc1p. Fmc1p is a yeast mitochondrial protein not found in higher eukaryotes. Tryptophan 94 (human) or 103 (yeast) is located in a positively charged region of Atp12p, and hence its mutation to arginine does not alter significantly the electrostatic properties of the protein. Instead, we provide evidence that the primary effect of the substitution is on the dynamic properties of Atp12p.

ATP is the principal energy source in cells. Eukaryotes make ATP from the cumulative activities of five multisubunit complexes that constitute the oxidative phosphorylation system of the inner membrane in mitochondria. In this process, the free energy of electrons liberated from oxidative metabolism of fuel molecules is harvested by complexes (I–IV) of the respiratory chain and converted to a transmembrane electrochemical proton gradient that fuels ATP synthesis catalyzed by complex V (ATP synthase) (1–3). ATP synthase is a large hetero-oligomer (~550 kDa) that can be resolved biochemically into two well defined protein entities called F_0 and F_1. F_1 is a soluble ATP hydrolase of 370 kDa and is composed of 3α and 3β, and 1 copy each of γ, δ, and ϵ subunits. Approximately 85% of the total mass of F_1 is contributed by the α and β subunits that occupy alternating positions in a hexameric ring, whereas the single copy subunits assemble an elongated structure that projects inside the hexamer (4–6). F_0 consists of a membrane-embedded proton pump and an extrinsic domain that serves as the attachment site for F_1. Whereas soluble F_1 is competent only for net ATP hydrolysis, the membrane-bound enzyme can utilize the energy released when protons translocate through F_0 to drive the endergonic reaction of ATP synthesis.

Nearly all of the proteins residing in mammalian mitochondria are the products of nuclear genes. Notable exceptions are the F_0 portions of the ATP synthase and three of the four respiratory chain proteins (complexes I, III, and IV), which are macromolecular structures assembled from the products of both nuclear genes and mtDNA (7, 8). This feature is responsible for the emergence of mtDNA in recent decades as an important target of investigation into the genetic basis for human diseases that show characteristics of defects in oxidative energy metabolism (7, 9). The T8993G/T8993C mutations in the mitochondrial gene *ATP6* for F_0 subunit a underlie the neurodegenerative pathologies associated with neurogenic ataxia retinitis pigmentosa and Leigh syndromes and are the best known genetic lesions linking a specific defect in ATP synthase to mitochondrial disease (10–12). Just recently, a mutation associated with mitochondrial disease was identified in *ATP8*, which is the other human F_0 gene of mitochondrial origin (13). An increasing number of patients are being identified for whom complex V deficiency is caused by a nuclear genetic defect (14), although none of the cases reported thus far identify a mutation in a nuclearly encoded F_1 or F_0 subunit. A recent paper by Cizkova *et al.* (15) reports the successful implementation of positional cloning to identify mutations in the human gene *TMEM70* associated with low levels of ATP synthase in a subpopulation of mitochondrial myopathy patients.

The model organism *Saccharomyces cerevisiae* has particular utility for the investigation of disease-linked mutations in nuclear genes associated with ATP synthase function. First is

* This work was supported, in whole or in part, by National Institutes of Health Grants GM69840 (to D. L. G.) and GM48157 (to S. H. A.). This work was also supported by Research Council of the Vrije Universiteit Brussel Grants OZR887 and ORZ1216, the Fund of Scientific Research-Flanders Grant FWO 6.06666.06, Agence Nationale de la Recherche grants, and the Association Française Contre les Myopathies grants (to J.-P. d. R.).

[1] Both authors contributed equally to this work.

[2] To whom correspondence should be addressed. Tel.: 313-577-8645; E-mail: sackerm@med.wayne.edu.

because yeast mutants have already identified a number of nuclear gene products that are imported by mitochondria for the sole purpose of mediating assembly of the ATP synthase (2). As several of these "assembly factors" share primary sequence homology with products of human genes, this information provides logical targets to investigate for genetic linkage to mitochondrial dysfunction originating in complex V. Work along these lines led De Meirleir *et al.* in 2004 (16) to identify the first nuclear defect linked to mitochondrial ATP synthase deficiency, which in this case occurred in the gene *ATPAF2* encoding a human homolog of the *S. cerevisiae* protein Atp12p that is required to assemble the F_1 oligomer (17). A second feature that highlights the value of yeast in studies of human mitochondrial disease becomes apparent when a human cDNA can be introduced into cells that are deficient for the homologous yeast protein and evaluated for an effect on respiration. Such considerations provide the basis for the experiments reported in this study, which have utilized yeast mutants to study a clinically isolated genetic variant of human *ATPAF2*.

Experiments in yeast have established that Atp12p binds to unassembled α subunits (18) and that this action is necessary to avoid off-pathway reactions leading to dead-end $(\alpha)_n$ aggregates (19). Complementation of the respiratory deficiency of yeast *atp12* mutants with a plasmid bearing wild type human *ATPAF2* cDNA has been already demonstrated (17). Furthermore, a deleterious effect of a specific Glu → Lys substitution, known to inactivate yeast Atp12p (hereon referred to as ScAtp12p), was recapitulated in human Atp12p (herein referred to as HuAtp12p) as determined by examination of recombinant HuAtp12p molecular chaperone activity *in vitro* using the model substrate citrate synthase (20).

This study was undertaken to determine the consequences of the W94R mutation in HuAtp12p that was reported by De Meirleir *et al.* (16) to cause severe complex V deficiency and patient death at age 14 months. Physical characterization of HuAtp12p(W94R), and related mutants (W94K, W94E, and W94A), revealed a defect in protein solubility. Molecular dynamics simulations of the wild type and HuAtp12p(W94R) protein provided an explanation at the atomic level for the solubility defect. Companion studies that evaluated the homologous mutation (W103R) in the context of yeast Atp12p indicate a universal relationship between this particular tryptophan residue and Atp12p solubility, which supports the marked conservation of the amino acid sequence at this position in the protein. Interestingly, although the defect in HuAtp12p(W94R) was readily apparent in the single deletion mutant Δatp12, it was necessary to create a strain (Δatp12Δfmc1) that is also missing the gene for Fmc1p to fully define the impact of the W103R substitution in ScAtp12p. Such findings provide new insight into the co-chaperone activity of Fmc1p that was first described by Lefebvre-Legendre *et al.* (21). This protein is not present in human mitochondria, which explains why it fails to suppress the deleterious effect of the W94R mutation in the human protein.

EXPERIMENTAL PROCEDURES

Yeast Strains and Growth Media—S. cerevisiae respiratory wild type strain, W303-1A (*MAT***a** *ade2-1 his3-11, 15 leu2-3, 112 ura3-1 trp-1*), and the derived respiratory-deficient mutant disrupted at the *ATP12* locus, **a**W303ΔG57, (*MAT***a** *ade2-1 his3-1, 15 leu2-3, 112 ura3-1 trp 1-1 ATP12*::*LEU2*), are described in Ref. 22. For simplicity, W303-1A is abbreviated as "W303" and **a**W303ΔG57 is referred to as "Δatp12" in this study. A haploid mutant harboring two disrupted alleles, *ATP12*::*LEU2* and *FMC1*::*HIS3*, was isolated from the progeny of **a**W303ΔG57 and the *MATα* strain MC6 (21) and named Δatp12Δfmc1 (*MAT***a** *ade2-1 his3-11, 15 leu2-3, 112 ura3-1 trp 1-1 ATP12*::*LEU2 FMC1*::*HIS3*). Plasmid-transformed yeast were maintained on minimal glucose (WO) medium (2% glucose, 0.67% yeast nitrogen base without amino acids) supplemented with amino acids and nucleotides as required. Rich media contained 2% peptone, 1% yeast extract, and one of the following carbons sources: 2% glucose (YPD), 2% galactose (Gal), or 2% ethanol + 3% glycerol (EG). Solid media contained 2% agar.

TABLE 1
Plasmids for human and *S. cerevisiae* Atp12p production in yeast

Name	Description	Ref.
$pHu12^{2\mu a}$	Wild type HuAtp12p, 2μ	17
pHu12(W94R)	HuAtp12p(W94R), 2μ	This study
pHu12(W94F)	HuAtp12p(W94F), 2μ	This study
pHu12(W94A)	HuAtp12p(W94A), 2μ	This study
pHu12(W94E)	HuAtp12p(W94E), 2μ	This study
pHu12(W94K)	HuAtp12p(W94K), 2μ	This study
$pSc12^{2\mu b}$	Wild type yeast Atp12p, 2μ	22
$pSc12_{CEN}$	Wild type yeast Atp12p, CEN	This study
$pSc12(W103R)^{2\mu}$	Yeast Atp12p(W103R), 2μ	This study
$pSc12(W103R)_{CEN}$	Yeast Atp12p(W103R), *CEN*	This study

[a] This plasmid was originally named pG13L/HUATP12(33–289).
[b] This plasmid was originally named pG57/ST4.

Plasmids and Site-directed Mutagenesis—A summary of the plasmids used to transform yeast is given in Table 1. Multicopy plasmids for production of wild type ScAtp12p ($pSc12^{2\mu}$ (formerly named pG57/ST4 (22)) and of HuAtp12p ($pHu12^{2\mu}$ (formerly named pG13L/HuATP12(33–289) (17)) are based in the 2μ *URA3*-bearing vector YEp352 (23). Following the manufacturer's instructions, QuikChange™ site-directed mutagenesis kit (Stratagene) was used with plasmid pHu12 to introduce the following amino acid substitutions in HuAtp12: W94R, W94F, W94E, W94A, and W94K, and with plasmid pSc12 to make a W103R substitution in the sequence for ScAtp12p. The sense strand of each pair of complementary oligonucleotides that was used for mutagenesis is given in Table 2. Plasmid inserts were sequenced to verify that only the desired mutations are present in the reading frames for the human and yeast Atp12p proteins. Single copy plasmids ($pSc12^{CEN}$, $pSc12(W103R)^{CEN}$) for the production of wild type and mutant ScAtp12p were made by transferring a 1.45-kb SacI-HindIII fragment from $pSc12^{2\mu}$ and from $pSc12(W103R)^{2\mu}$, respectively, to the *URA3*-bearing *CEN* vector pRS316.

Electron Microscopy—Fibroblasts were washed with 0.1 M sodium cacodylate buffer, pH 7.4, and fixed in 0.4% glutaraldehyde, 4% paraformaldehyde in culture flasks. The cells were collected by centrifugation at 1717 × *g*, 5 min, at room temperature and pellets were incubated in fixative for another hour at 4 °C. Samples were post-fixed in osmium tetroxide (1% in buffer), dehydrated in a series of alcohol baths, and embedded in Epon (Aurion, Wageningen, The Netherlands). Ultrathin sections of 60 nm were examined using a Zeiss TEM900 trans-

TABLE 2
Primers for QuikChange™ site-directed mutagenesis[a]

Mutation	Primer[b]	Position in HuAtp12p cDNA
W94A	5'-CCATTGCAGTtGCTACTGAGgcGGATTCCCAGCAG-3'	260-294
W94E	5'-CCATTGCAGTtGCTACTGAGgaGGATTCCCAGCAG-3'	260-294
W94F	5'-CCATTGCAGTtGCTACTGAGTt t GATTCCCAGCAG-3'	260-294
W94K	5'-CCATTGCAGTtGCTACTGAGaaGGATTCCCAGCAG-3'	260-294
W94R	5'-CCATTGCAGTtGCTACTGAGagGGATTCCCAGCAG-3'	260-294
		Position in yeast Atp12p DNA
W103R	5'-GCATACCTATTAAAACTcGAGtGGTCGTCCCTATCCAGTC-3'	286-325

[a] Only the DNA sequence for the forward primer ("sense strand") is shown; the reverse primer is the complementary sequence.
[b] Nucleotide changes to the wild type sequences are in lowercase letters. Codon changes are highlighted in gray. Silent substitutions are underlined.

mission electron microscope at 50 kV and magnification at ×20,000. A total of 30 micrographs were recorded for three different fibroblast cell samples collected from the patient described in Ref. 16. Mitochondria were counted, and cristae morphology (normal and aberrant) and matrix density (lucent, intermediate, and dense) were assessed in a blinded fashion, and cross-tabs were performed together with χ^2 tests (data not shown).

Homology Modeling of HuAtp12p—A homology model of HuAtp12p was built with Prime 2.1 (Schrödinger Inc.) using as a template the x-ray structure of *Pseudomonas denitrificans* Atp12p (24). First, an optimal sequence alignment was identified between the query sequence and the template, and then a secondary structure prediction on the query sequence was used to further improve the alignment. Finally, the entire structure of the query sequence was built in sequential steps as follows: (*a*) coordination of the copying of backbone atoms for aligned regions and side chains of conserved residues; (*b*) building insertions and closing deletions in the alignment; (*c*) building tails out to the last residue in the template; (*d*) side chain prediction of nonconserved residues; and (e) minimization of all the atoms not derived directly from the template. The final homology model included residues 33–277 of human Atp12p. There is no equivalent for residues 1–32 in *P. denitrificans* Atp12p, suggesting that these residues probably represent the mitochondrial import leader peptide of the human protein. The root mean square deviation (r.m.s.d.)[3] for 177 out of 227 Cα of the human protein model with respect to *P. denitrificans* Atp12p is 1.775 Å. The other Cα atoms (mostly corresponding to loop regions) have r.m.s.d. values not exceeding 4.05 Å. HuAtp12p was solvated in a cubic box of SPC water (25) molecules with Desmond (D. E. Shaw Research) (26) leaving a minimum distance of 12 Å between any protein atom and the edge of the box. The W94R variant of HuAtp12p was generated by replacing the tryptophan side chain with an arginine side chain using Maestro (Schrödinger Inc.) and repeating the energy minimization.

Molecular Dynamics—The ensembles of the wild type and the mutant HuAtp12p, each consisting of ~55,000 atoms representing the protein, 17,084 water molecules, and 5 to 6 sodium ions neutralizing the protein charges, were then subjected to steepest descent minimization under periodic boundaries condition until a gradient threshold of 25 kcal/mol/Å was reached, followed by limited-memory Broyden-Fletcher-Goldfarb-ShannoLBFGS minimization (27, 28). The 2005 release of the optimized potentials for liquid simulations (all atom) force field (29) was used in this and all subsequent calculations. Short range Coulombic interactions were calculated with a cutoff radius of 9.0 Å, whereas long range interactions were calculated with the smooth particle mesh Ewald method (30) using an Ewald tolerance of $1e^{-9}$. A 40-ns MD simulation was carried out with Desmond in the number-pressure-temperature ensemble at 300 K (25 °C). For this purpose, the Nose-Hoover thermostat method (31) with a relaxation time of 1.0 ps and the Martyna-Tobias-Klein barostat method (32) with isotropic coupling of the cell along all three axes to a reference pressure of 1.01325 atm and a relaxation time of 2 ps were used. Integration was carried out with the RESPA integrator (33) using time steps of 2.0, 2.0, and 6.0 fs for the bonded van der Waals and short range and long range electrostatic interactions. SHAKE constraints (34) were imposed on all the heavy atom-hydrogen covalent bonds. Coulombic interactions were calculated as for the minimization protocol. Coordinates were saved every 4.8 ps. Before the 40-ns productive run of the simulation, the ensemble was relaxed using the following protocol: 1) 12 ps in the number-volume-temperature ensemble at 10 K with a fast relaxation constant and non-hydrogen solute atoms restrained; 2) 12 ps in the number-pressure-temperature ensemble at 10 K and 1 atm, with a fast temperature relaxation constant, a slow pressure relaxation constant, and non-hydrogen solute atoms restrained; 3) 24 ps at 300 K and 1 atm with other conditions as in step 2; and 4) 24 ps at 300 K and 1 atm with a fast temperature relaxation constant and a fast pressure relaxation constant.

Electrostatic Potentials and Energy Calculations—Electrostatic potentials at the solvent-accessible surface of proteins and solvation energies were calculated with PDB2PQR/APBS (35) using a nonlinear Poisson-Boltzmann continuum model with a solvent dielectric constant $\epsilon_s = 78$. A protein dielectric

[3] The abbreviations used are: MD, molecular dynamics; r.m.s.d., root mean square deviation; r.m.s.f., root mean square fluctuation; HMM, Hidden Markov Model.

constant $\epsilon_p = 10$ was adopted (instead of the traditional $\epsilon_p = 2$), as recommended by several authors (36–38) to avoid artificially high values of the polar solvation energy terms. Protein charges were assigned on the basis of the AMBER force field (39), assuming a pH of 8.0 for the mitochondrial matrix (40), and by calculating the pK_a values of all ionizable residues with the program PROPKA (41).

All energy calculations were carried out on fixed conformations of Atp12p, derived from the MD simulation at 300 K. As these calculations do not include entropic and molecular mechanics energy changes, the calculated solvation energies of the states are to be considered as "potentials of mean force" rather than free energies. The solvation energy of each individual state was calculated as the sum of two components that describe a thermodynamic cycle in terms of transfer energies from a homogeneous dielectric environment (where interactions are described by Coulomb's law) to an inhomogeneous dielectric environment with differing internal and external dielectric constants. The first component includes the polar solvation term. For this calculation, we used a grid of ~0.5-Å spacing covering the entire protein. The second component, represented by the apolar solvation energy, was modeled according to Wagoner and Baker (42) using the "probe-inflated" model of the solvent-accessible surface and volume. Key parameters were as follows: solvent pressure, 0.150624 kJ mol^{-1} Å^{-3}; repulsive solvent surface tension, 0.012552 kJ mol^{-1} Å^{-1}; bulk solvent density, 0.033428 Å^{-3}; solvent molecule radius, 1.04 Å. Figs. 6 and 8 were generated with PyMOL (43).

Miscellaneous Methods—Preparation of mitochondria, denaturing (SDS) gels, and Western analysis was as described previously (18). Polyclonal antibodies raised against denatured ScAtp12p were used at 1:1000 dilution to detect both yeast and human Atp12p proteins in Western blots (20). The LiAc method of Schiestl and Gietz (44) was used to transform yeast. Protein concentration was measured according to Lowry *et al.* (45).

RESULTS

Probing the Effect of HuAtp12p(W94R) on Mitochondrial Ultrastructure in Human Fibroblast Cells—Fibroblast cells cultured from the HuAtp12p(W94R) patient described in Ref. 16 were embedded in epoxy resin and analyzed by transmission electron microscopy (Fig. 1). Cells were stained with osmium tetroxide, post-fixation, to achieve the high contrast necessary to discern mitochondrial ultrastructure without further labeling. There were no significant differences in cristae morphology or matrix density between the patient and control cells (Fig. 1, compare *panels A* and *B* with *C* and *D*). This finding is different from what was reported in transmission electron micrographs of Atp12p-deficient yeast stained with OsO_4, which showed clear evidence of electron-dense material inside mitochondria that was identified to be deposits of aggregated F_1 α and β subunit proteins by immunogold labeling (46). Although our results show no evidence of such structures in the fibroblast cells from the patient, we cannot rule out the possibility that an aggregated F_1 protein phenotype may have been lost with repeated passage of the cells in culture. The resolution of this issue awaits the availability of fresh tissue from new patients diagnosed with HuAtp12p deficiency.

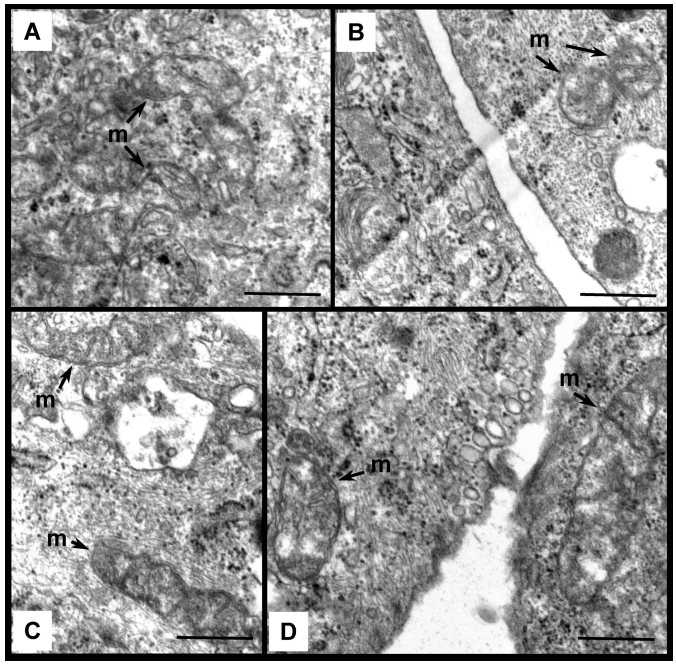

FIGURE 1. **Ultrastructural analysis of human fibroblasts from HuAtp12p(W94R) patient.** Transmission electron micrographs of Epon 60-nm-thick sections of fibroblasts cultured from the HuAtp12p(W94R) patient (*panels A* and *B*) and control source (*panels C* and *D*). *m*, mitochondria. *Bars*, 0.5 μm.

TABLE 3

Mitochondrial ATPase activities of yeast that produce W94^{Hu}/W103^{Sc} Atp12p mutants

Strain	ATPase activity[a]	
	−Oligomycin	+Oligomycin
	μmol of P_i released/min/mg	
Wild type	3.79 ± 0.40	0.44 ± 0.11
Δatp12	0.24 ± 0.07	0.05 ± 0.06
Δatp12 + pHu12$^{2\mu}$	2.37 ± 0.06	0.16 ± 0.02
Δatp12 + pHu12(W94R)	0.22 ± 0.03	0.07 ± 0.08
Δatp12 + pHu12 (W94F)	2.37 ± 0.54	0.19 ± 0.11
Δatp12 + pHu12 (W94A)	0.20 ± 0.06	0.06 ± 0.03
Δatp12 + pHu12 (W94E)	0.20 ± 0.01	0.18 ± 0.12
Δatp12 + pHu12 (W94K)	0.30 ± 0.08	0.03 ± 0.04
Δatp12 + pSc12$^{2\mu}$	2.98 ± 0.16	0.34 ± 0.09
Δatp12 + pSc12(W103R)$^{2\mu}$	2.63 ± 0.83	0.25 ± 0.03
Δatp12 + pSc12^{CEN}	3.23 ± 0.06	0.38 ± 0.05
Δatp12 + pSc12(W103R)^{CEN}	2.71 ± 0.76	0.25 ± 0.08

[a] Mitochondrial ATPase activity was measured at 37 °C by the colorimetric determination of P_i released as described (53). The mean values from two independent assays ± S.D. reported.

Nonconservative Substitutions of Trp-94 in HuAtp12p Cause Respiratory Deficiency in Yeast—The multicopy yeast plasmid pHu12$^{2\mu}$ (Table 1) encodes a chimeric protein in which a *bona fide* yeast mitochondrial leader sequence replaces the native targeting sequence (first 32 codons) of HuAtp12p. Introduction of this plasmid into the yeast deletion strain Δatp12 confers the mutant with high levels of oligomycin-sensitive ATPase activity (Table 3) and respiratory growth on nonfermentable carbons (ethanol-glycerol, EG media) (17). To study effects of the W94R mutation on mitochondrial function in the yeast model, the QuikChange method was used to substitute Arg for Trp-94 in the HuAtp12p sequence carried on pHu12$^{2\mu}$ (see under "Experimental Procedures"). The re-

sultant plasmid pHu12(W94R) failed to confer respiratory competence to Δatp12 as indicated by the EG− phenotype of the transformed yeast (data not shown). In addition, there was no oligomycin-sensitive ATPase activity detected in mitochondria isolated from the transformant (Table 3).

Four additional mutant plasmids were created to investigate the stringency in amino acid sequence at position 94 in HuAtp12p by substituting the tryptophan with alanine, glutamate, lysine, or phenylalanine (Table 1). Among these plasmids, only pHu12(W94F) complemented the respiratory defect of Δatp12, converting the strain to an EG+ phenotype and restoring oligomycin-sensitive ATPase activity to the same level as that observed for transformants bearing the wild type HuAtp12p plasmid (Table 3). The other three plasmids (pHuATP12(W94A, W94E, and W94K)) were all completely deficient in this respect. The trend in our results was in accordance with the fact that when aligned with multiple Atp12p sequences from diverse genetic backgrounds, Trp-94 of the human protein is conserved as either Trp or Phe (see under "Discussion").

W94R Mutation Decreases the Solubility of HuAtp12p—A principal objective in this work was to extend the assays developed for *in vitro* analysis of recombinant HuAtp12p (20) to the W94R mutant protein. Plasmid pPROEX/Atp12ph, which produces the leaderless intramitochondrial form of wild type HuAtp12p in *Escherichia coli* (20), served as the template for QuikChange mutagenesis with the same primers used to create pHu12(W94R) (see Table 2 and above), and the new expression vector (pPROEX/Atp12ph(W94R)) was used to transform *E. coli*. The method described by Hinton *et al.* (20) for bacterial overproduction of wild type and E240K mutant HuAtp12p yields ~70% recombinant protein recovered in the soluble fraction from broken cells. However, under the established conditions, HuAtp12p(W94R) forms inclusion bodies in bacteria. Given the clinical relevance of the W94R substitution in HuAtp12p, a significant effort was made to modify various aspects of the protocol to provide us with the mutant protein in a soluble form. The major variables manipulated included isopropyl β-D-thiogalactopyranoside induction time (1–24 h), induction temperature (15, 23, 30, and 37 °C), 2% ethanol supplementation (47), and *E. coli* host strain (JM109 and BL21). With one exception, recombinant HuAtp12p(W94R) partitioned completely to the insoluble fraction under the conditions tested; representative examples are shown in Fig. 2*A*. JM109 transformants induced for 6–12 h at 15 °C, minus ethanol, gave the most promising results (Fig. 2*A*, *2nd set* from the *right*). However, despite multiple attempts to optimize the method (*e.g.* Fig. 2*B*), we were unable to prepare His tag-HuAtp12p(W94R) from JM109 extracts in amounts sufficient for *in vitro* studies. The striking difference of these results *versus* previous work with wild type and E240K HuAtp12p recombinant proteins (20) suggested that the primary impact of the mutation was a change in physical rather than functional parameters.

Ability of Plasmid-borne ScAtp12p(W103R) to Confer Respiratory Function to Δatp12 Yeast Is Dependent on Fmc1p—In contrast to what we found for HuAtp12p(W94R), a plasmid coding for the yeast protein bearing the homologous mutation

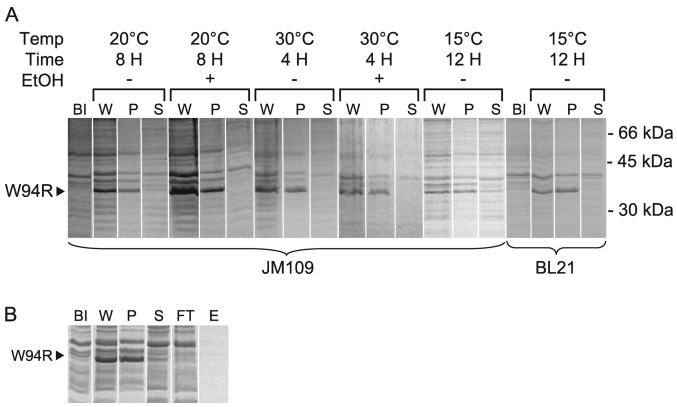

FIGURE 2. **Behavior of recombinant HuAtp12(W94R) in bacterial cell fractions.** *Panel A*, small scale expressions from pPROEX/Atp12ph(W94R) in bacteria. Transformed cells (*JM109* and *BL21*) were cultured overnight at 30 °C in 2× YT (1.6% bacto tryptone, 1% yeast extract, 0.5% NaCl, pH 7.0), supplemented with ampicillin (50 μg/ml), diluted into 10 ml of fresh media the next morning, and grown to mid-log phase in 50-ml flasks. A sample (1 ml) was removed before induction (*BI*), after which the cultures were brought to 1 mM isopropyl β-D-thiogalactopyranoside and, where indicated, 2% ethanol, and incubated under the conditions for time and temperature specified for each experiment. Cells were collected by centrifugation and suspended in 1 ml of 20 mM Tris-HCl, pH 7.5; a sample (20 μl) of whole cells (*W*) was removed, and the remainder was exposed to sonic irradiation to break the cells. The sonicated material was centrifuged at 13,000 × *g* for 2 min; the supernatant (*S*) was collected, and the pellet (*P*) was suspended in 20 mM Tris-HCl, pH 7.5, to the original volume. Aliquots of the cells before induction, and post-induction whole cell, supernatant, and pellet samples were brought to 1× gel loading buffer and applied (10 μl) to 12% SDS-polyacrylamide gels. Gels were stained with Coomassie Blue R-250. The migration of HuAtp12p(W94R) (*arrowhead*) relative to molecular weight standards (*right*) is shown. *Panel B*, large scale expression from pPROEX/Atp12ph(W94R) in bacteria. Transformed JM109 cells were induced with 1 mM isopropyl β-D-thiogalactopyranoside in 2 liters of 2× YT + ampicillin for 8 h at 15 °C. The cells were then collected by centrifugation at 5000 × *g* for 5 min at 4 °C, suspended in 25 ml of breaking buffer (20 mM Tris-HCl, pH 7.5, 0.2 mg/ml lysozyme, 0.01% phenylmethylsulfonyl fluoride), and broken by passing through a French press three times. Streptomycin sulfate was added (1%) to precipitate DNA, and the broken cells were centrifuged at 100,000 × *g* for 1 h. The supernatant was filtered through a 0.2-μm membrane, diluted to 80 ml, and applied to a 10-ml TALON® cobalt-chelate resin column (Clontech). The column was washed with 120 ml of 20 mM Tris-HCl, pH 7.5, and eluted with 20 ml of the buffer supplemented with 0.2 M imidazole. Samples of cells before induction (*BI*) and after breaking (whole cell (*W*), pellet (*P*), and supernatant (*S*)) and the flow-through (FT) and eluate (*E*) from the cobalt column were analyzed in SDS gels as described for *panel A* above.

(ScAtp12p(W103R)) was shown to confer an EG+ phenotype to Δatp12, even when produced from a single copy plasmid (data not shown). Moreover, the amount of oligomycin-sensitive ATPase supported by ScAtp12p(W103R) was determined to be >60% of the wild type level (Table 3, see data for $pSc12^{CEN}$ and $pSc12(W103R)^{CEN}$), which is well above the 15% threshold that is necessary for yeast to grow on EG plates (48). Western blots of mitochondrial fractions provided key information about the contrasting abilities of HuAtp12p(W94R) and ScAtp12p(W103R) to rescue Δatp12 yeast (Fig. 3). Mitochondria from respiratory wild type yeast (W303), untransformed Δatp12, and plasmid-bearing Δatp12 were exposed to mild treatment with sodium deoxycholate and centrifuged at 100,000 × *g* for 30 min. Under these conditions, ~75% ScAtp12p was recovered in the supernatant fraction (Fig. 3, *panel A, W303*), which is in accord with results obtained when yeast mitochondria are disrupted by sonic irradiation (22, 49). For reference, a Western blot is included here (Fig. 3, *panel A*, Δ*atp12*) to show the nonspecific cross-reactivity of the anti-

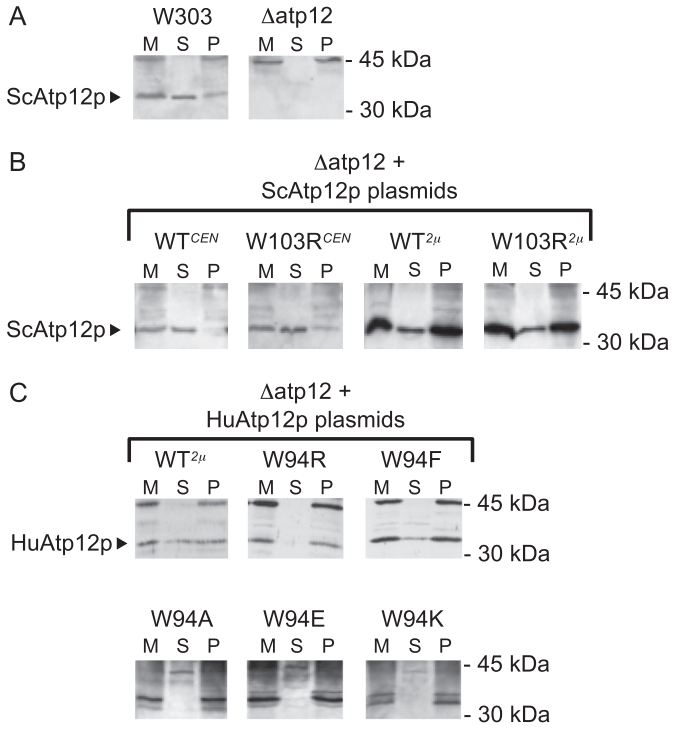

FIGURE 3. **Western blot analysis of wild type and mutant Atp12p in mitochondria.** Mitochondria were prepared from yeast cells grown in GAL media as described previously (53) and suspended to 10 mg/ml in 0.3 ml of 20 mM Tris-HCl, pH 8.0, and sodium deoxycholate was added to 0.1% to permeabilize the membranes. An aliquot of total mitochondria (*M*) was removed, and the rest of the sample was centrifuged at 100,000 × *g* for 1 h at 4 °C. The supernatant (*S*) was collected, and the pellet (*P*) was resuspended to the original volume in the same buffer. Samples of mitochondria (50 μg) and equivalent volumes of the supernatant and pellet fractions were resolved on a 12% SDS-polyacrylamide gel, and following the transfer of proteins to nitrocellulose membranes, Western analysis was done using polyclonal antibody against ScAtp12p (see "Experimental Procedures"). *Panel A*, isogenic wild type (*W303*) and *ATP12*::*LEU2* disruption strain (Δ*atp12*). *Panel B*, Δatp12 bearing single (*CEN*) or multicopy (2μ) plasmid for wild type or W103R ScAtp12p. *Panel C*, Δatp12 bearing multicopy plasmid for wild type or W94-substituted HuAtp12p. The migration of Atp12p is shown by the *arrowhead*. The positions of molecular mass standards are shown on the *right*.

ScAtp12p serum *versus* mitochondrial samples from untransformed Δatp12. Comparing separately the results obtained using either single copy (*CEN*) or multicopy (2μ) ScAtp12p plasmids, wild type and W103R mutant proteins were detected in similar amounts in whole mitochondria and showed comparable partitioning behaviors following permeabilization and fractionation of mitochondria (Fig. 3, *panel B*). The finding that most of the ScAtp12p is recovered in the particulate fraction when the protein is overproduced from a 2μ plasmid is typical of the system and may suggest the titration of another protein(s) that determines the solubility of Atp12p in yeast mitochondria. Antibodies against ScAtp12p cross-react with purified recombinant HuAtp12p (20) and were shown here to detect the wild type human protein produced from a multicopy plasmid in yeast mitochondrial samples (Fig. 3, *panel C, WT*). It was necessary to do these experiments with mitochondria from multicopy Δatp12/HuAtp12p transformants, even though the Δatp12 respiratory defect is rescued by a single copy HuAtp12p plasmid (data not shown), to detect the protein in Western blots with anti-ScAtp12p serum. Notwithstanding the artificial increase in gene copy number, there was no evidence of plasmid-encoded mutant Atp12p in soluble mitochondrial fractions from pHuW94R-transformed cells (Fig. 3, *panel C, W94R, lane S*), although the protein was detected in total mitochondria and submitochondrial particulate fractions from these cells (*panel C, W94R, lanes M* and *P*). Consistent with the functional analysis of the other HuAtp12p mutants described above, only the W94F protein was detected in Western blots of soluble extracts of yeast mitochondria (Fig. 3, *panel C*). Instead, cross-reacting protein approximately the size of HuAtp12p was observed in only the mitochondrial and submitochondrial particulate fractions from yeast that produce W94A, W94E, or W94K mutant proteins.

Western analysis suggested that the contrasting results from Δatp12 complementation experiments with HuAtp12p(W94R) and ScAtp12p(W103R) plasmids might be due to an aberrant conformation of the human protein in mitochondria. Such considerations prompted investigation into the effects of another mitochondrial protein (Fmc1p) that is associated with Atp12p-mediated F_1 assembly in yeast cells (21). Yeast Δfmc1 cells change from an EG+ to an EG− phenotype when the temperature of the growth medium is increased from normal (30 °C) to 37 °C, and the conditional phenotype is rescued by supplying excess ScAtp12p from a plasmid (21). Mitochondria isolated from Δfmc1 (MC6) yeast cultured at 37 °C are deficient for mitochondrial ATPase activity, and almost no ScAtp12p is detected in Western blots of these samples (21). Even when cells are grown at 30 °C, the amount of ScAtp12p is greatly reduced in Western blots of mitochondria isolated from MC6 *versus* the isogenic wild type strain (MC1) (data not shown). Hence, although Δfmc1 cells passed the screen for respiratory competence at 30 °C, there was already evidence that the function of wild type ScAtp12p was compromised under these conditions. On this basis, we decided to evaluate the effect of the W103R mutation in yeast cells depleted for the accessory protein Fmc1p. Double mutant haploid progeny (Δatp12Δfmc1) were isolated from a cross of the relevant parental strains (see "Experimental Procedures"), transformed with plasmids for the production of wild type and W103R mutant ScAtp12p, and evaluated for respiratory function and mitochondrial ATPase activity. Untransformed Δatp12Δfmc1 grew well on a fermentable carbon source (glucose, YPD plates) at 30 °C, but was compromised in this capacity at 37 °C (Fig. 4, *uppermost panels*). In this respect the double mutant was similar to the parental strains, Δatp12 and Δfmc1, both of which show growth defects on YPD at elevated temperature (data not shown). The experiments on nonfermentable media (ethanol-glycerol, EG plates) took advantage of an important difference between the parental strains; Δatp12 is completely EG− at all temperatures (50), whereas Δfmc1 cells are EG+ at 30 °C and EG− at 37 °C (data not shown, see above). Hence, the double mutant should grow on EG plates at 30 °C if provided with a functional form of ScAtp12p encoded on a plasmid. We show here that ScAtp12p conferred respiratory function to Δatp12Δfmc1 at 30 °C when supplied on a single copy plasmid (Fig. 4, *lower, pSc12*^{CEN}). Moreover, double mutant cells that overproduce wild type ScAtp12p showed evidence of respiratory activity at 37 °C (Fig. 4, *lower, pSc12*$^{2\mu}$), although rescue of the temperature-sensitive phenotype was less robust than observed with plasmid-borne

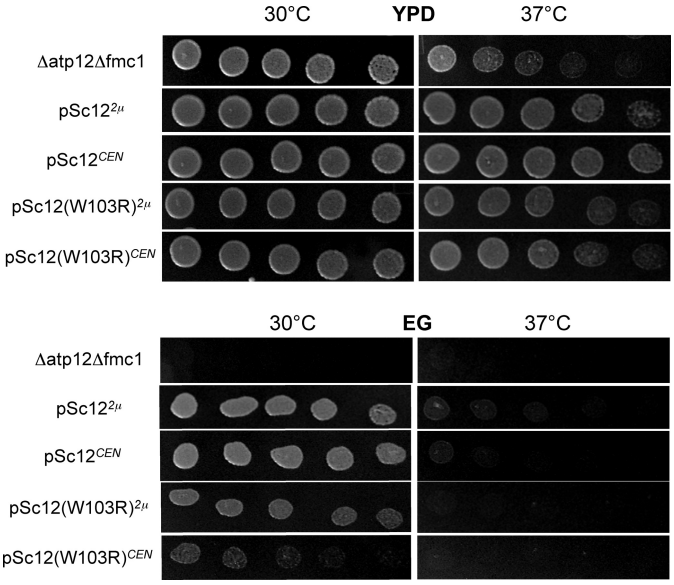

FIGURE 4. **Growth of *S. cerevisiae* mutants on fermentable and nonfermentable carbons.** Δ*atp12*Δ*fmc1*, both untransformed and transformed with either a multicopy or a single copy plasmid for wild type or mutant ScAtp12p (*pSc12*$^{2\mu}$, *pSc12*^{CEN}, *pSc12*(*W103R*)$^{2\mu}$, *pSc12*(*W103R*)^{CEN}), was tested for growth on glucose (YPD) and nonfermentable ethanol glycerol (EG) plates at 30 or 37 °C. Following overnight growth in liquid YPD, cell cultures were adjusted to $A_{600} = 1.0$, and then serially diluted by a factor of 2. Five μl of each dilution were applied to plates that were incubated at the indicated temperature for 48 h.

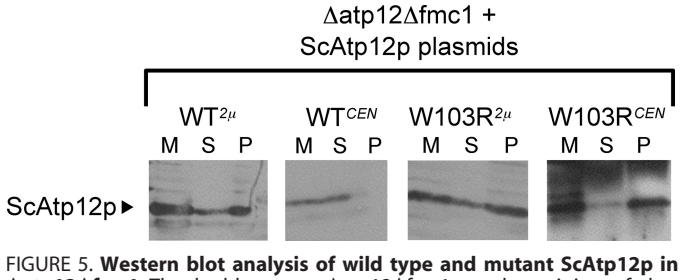

FIGURE 5. **Western blot analysis of wild type and mutant ScAtp12p in Δatp12Δfmc1.** The double mutant Δatp12Δfmc1 was the recipient of plasmids for ScAtp12p. All other aspects of this figure are as described in Fig. 3, *panel B*. *M*, mitochondria; *S*, supernatant; *P*, pellet.

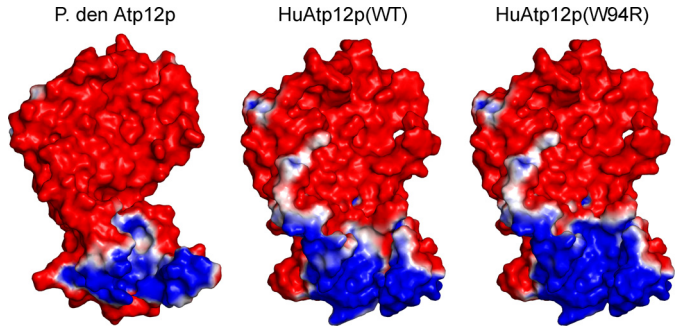

FIGURE 6. **Homology models of wild type (*WT*) and W94R mutant HuAtp12p.** Proteins are colored according to the electrostatic potentials (+1 *kT*/e, *blue*; −1 *kT*/e, *red*) at the solvent-accessible surface.

TABLE 4

Atp12p(W103R) is dependent on Fmc1p to support mitochondrial ATPase activity in yeast

Strain	ATPase activity[a]	
	−Oligomycin	+Oligomycin
	μmol P_i released/min/mg	
Wild type	1.60 ± 0.32	0.40 ± 0.02
Δatp12Δfmc1	0.42 ± 0.01	0.27 ± 0.02
Δatp12Δfmc1 + pSc12$^{2\mu}$	1.50 ± 0.10	0.58 ± 0.02
Δatp12Δfmc1 + pSc12(W103R)$^{2\mu}$	1.14 ± 0.15	0.25 ± 0.07
Δatp12Δfmc1 + pSc12^{CEN}	1.88 ± 0.10	0.96 ± 0.15
Δatp12Δfmc1 + pSc12(W103R)^{CEN}	0.26 ± 0.12	0.17 ± 0.09

[a] Mitochondrial ATPase activity was measured at 30 °C spectrophotometrically by following NADH depletion in a coupled enzyme assay as described (53). The mean values from two independent assays ± S.D. are reported.

ScAtp12p in the simple mutant Δfmc1 (21). The growth phenotypes were significantly different for Δatp12Δfmc1 cells carrying plasmids for the mutant protein. Multicopy plasmid transformants (Fig. 4, *pSc12*(*W103R*)$^{2\mu}$) were EG− for the first 24–36 h at 30 °C and remained completely EG− at 37 °C, even following extended incubation (data not shown). Moreover, the single copy plasmid pSc12(W103R)^{CEN} barely conferred respiratory function following 48 h at the permissive temperature (Fig. 4, *30 °C, lower left-most panel*). The results from mitochondrial ATPase activity assays were in accord with the growth analysis on EG plates (Table 4). Comparable oligomycin-sensitive ATPase was measured for transformants bearing multicopy or single copy plasmids for wild type ScAtp12p. In contrast, there was essentially no mitochondrial ATPase activity measured for samples from Δatp12Δfmc1 cells carrying a single copy plasmid (pSc12(W103R)^{CEN}) for the mutant protein. It is worth noting that we observed a higher level of oligomycin-insensitive ATPase when pSc12^{CEN} was introduced in Δatp12Δfmc1 *versus* the simple mutant Δatp12 (compare data in Tables 3 and 4). The significance of this finding remains unknown.

W103R Mutation Decreases the Solubility of ScAtp12p—The Δatp12Δfmc1 transformants provided the opportunity to assess the innate properties of wild type and W103R mutant ScAtp12p (Fig. 5). Experiments with the single copy (*CEN*) plasmids were most informative as these show a significant difference in the way wild type and W103R mutant proteins partition to soluble and particulate fractions following the permeabilization of mitochondria. On its own, the wild type protein is soluble, whereas ScAtp12p(W103R) mirrors the defect observed in HuAtp12p(W94R).

Solution Properties of Wild Type and W94R Mutant HuAtp12p as Determined by Molecular Dynamics Simulations—The physical properties of the wild type and W94R mutant HuAtp12p in solution were investigated by means of MD simulations in the number-pressure-temperature (constant pressure and temperature) ensemble with structural models for all atoms built using the 1.0 Å x-ray structure of *P. denitrificans* Atp12p (Protein Data Bank entry 2R31) (24) as a template as described under "Experimental Procedures." Because of the differences in many side chains, the solvent-accessible surface of the human protein appears slightly "bulkier" than its bacterial counterpart (Fig. 6). The structures of wild type and W94R mutant HuAtp12p are essentially identical, although there is a small difference in the electrostatics of the "wrist" domain (as defined in Ref. 24), due to the introduction of the positively charged arginine (Fig. 6).

MD simulations were carried out at 300 K (25 °C), and trajectories were recorded for 40 ns with frames every 4.8 ps. During the course of the MD simulation, both the wild type and W94R mutant HuAtp12p progressively deviate from their ini-

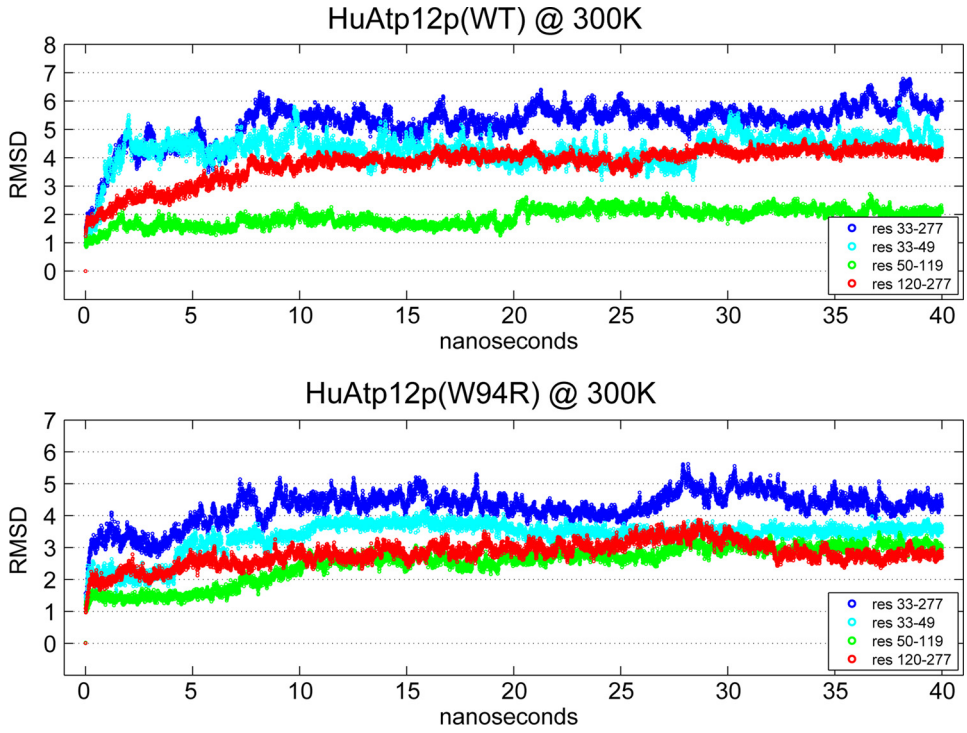

FIGURE 7. **MD simulations of wild type (*WT*) and W94R mutant HuAtp12p.** Cα-r.m.s.d. (*RMSD*) values (Å) of each frame at time *t* with respect to the frame at time $t = 0$ were calculated for the wrist (residues 33–119) and the palm (residues 120–277) domains. The contribution from the wrist domain was further broken down into residues 33–49, where the largest conformational differences between wild type and W94R occur, and residues 50–119.

TABLE 5

r.m.s.f. fluctuations (Å) of wild type and W94R HuAtp12p during the final 20 ns of MD simulation

	Wrist domain						Palm domain	
	Residues 33–119	S.D.[a]	Residues 33–49	S.D.	Residues 50–119	S.D.	Residues 120–277	S.D.
Wild type	2.2395	0.4275	2.444	0.767	0.9595	0.152	1.403	0.192
W94R	1.607	0.2465	0.684	0.229	1.146	0.219	1.3325	0.2555

[a] S.D., standard deviation.

tial conformation (the homology model) until they reach an equilibrium after ~15 ns (Fig. 7). The different values at equilibrium of the Cα-r.m.s.d. of the wild type and W94R mutant proteins with respect to $t = 0$ reflect how different each of the solution structures are from the initial homology models shown in Fig. 6. It is important to notice that this very long equilibration time progressively eliminates possible errors in the original models and ensures that the average structure of the two proteins at equilibrium is as close as possible to their true native structure in solution. The final part of the simulation (20–40 ns) was selected to gather statistics about the conformational properties of the two proteins. The fluctuations around the average structure (Cα root mean square fluctuation, Cα-r.m.s.f.) that occur in this part of the simulation reflect the degree of mobility in the solution structure. r.m.s.f. values and standard deviations for the wrist and palm domains of Huatp12p are shown in Table 5.

The palm domain (residues 120–277) displays similar fluctuations (r.m.s.f. of 1.4 and 1.33) in both the wild type and the W94R mutant protein. In contrast, the wrist domain (residues 33–119) is significantly more mobile in the wild type protein (r.m.s.f. of 2.24 *versus* 1.61). A break down of the contributions to the wrist domain fluctuations originating from residues 33 to 49 and from residues 50 to 119 shows that most of the Cα-r.m.s.f. differences are due to the significantly higher mobility of the first 17 residues of the wrist domain. These differences were investigated further with a clustering procedure (incorporated in the program X-Cluster, Schrodinger Inc.) that, based on the cross-r.m.s.d. values between 417 frames (1 every 10 of the original 4168 frames in the 20–40-ns interval), identified the three structures most representative of all the states sampled during the molecular dynamics run, which thus can be considered as fluctuations around these three main conformations. The three representative configurations of the wild type protein appear in the simulation in a 239:177:1 relative ratio; the three W94R configurations appear in a 401:14:2 relative ratio (Fig. 8). In the wild type protein, residues 33–49 are extended outward and the hydrophobic cavity harboring Trp-94 is narrowed. In the W94R mutant protein, the hydrophobic cavity opens up, and residues 33–49-fold back into it. It is also worth noting that in the mutant the angle between the wrist and the palm domain is more acute than in the wild type, and as a consequence the overall structure of HuAtp12p(W94R) appears more compact than the wild type (Fig. 8).

Altogether, these differences dramatically alter the solvent-accessible surface of the two proteins and affect their solvation properties. Solvation energies (broken down in their polar and nonpolar components), calculated for the three most representative conformations of the wild type and W94R mutant protein, are listed in Table 6. The W94R mutant is associated with a significantly more positive solvation energy in all the configurations. Furthermore, when all three configurations are weighted by their relative contribution to the population of states in solution as determined from the MD run, an average $\Delta\Delta G_{\text{W94R-WT}} = 232.03 - (-42.06) = 274.09$ kcal/mol is derived. Although the current state of theory for the computation of solvation energies does not provide assurance that the absolute numbers are without errors, the relative trends in solvation energies and the corresponding differences are considered reliable, and in this particular case they suggest that the mutant protein is less soluble than the wild type (in agreement with the experimental observations discussed above).

DISCUSSION

The W94R mutation in HuAtp12p was identified as the causative factor for ATP synthase deficiency underlying a fatal mito-

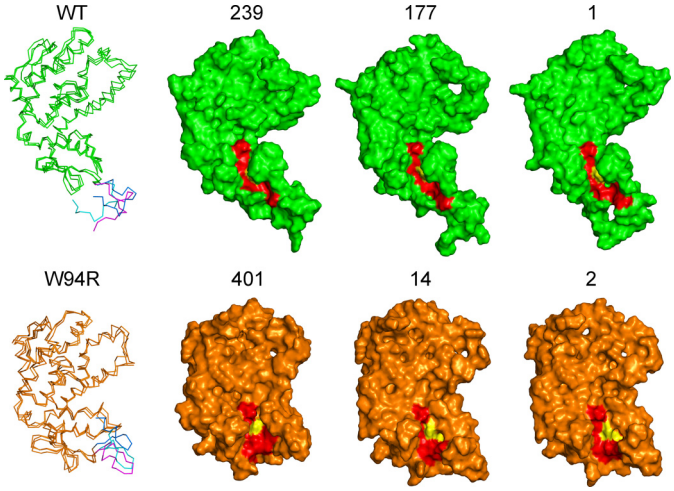

FIGURE 8. **Representative conformations of wild type (*WT*) and W94R mutant HuAtp12p observed in the equilibrium phase (20–40 ns) of an MD simulation at 300 K.** Wild type and W94R mutant proteins are shown, respectively, in the *upper* and *lower panels*. The *leftmost panels* show a superposition of the three most representative conformations. The three conformations of residues 33–49 are shown in *blue, magenta,* and *cyan*. The other panels show the solvent-accessible surface of the wild type and W94R protein in the three conformations. The surface of a hydrophobic groove in the wrist domain is shown in *red*. The surface corresponding to Trp-94 or Arg-94 is shown in *yellow*. The relative contributions of the three conformations to the ensemble in solution in indicated above the surfaces.

TABLE 6

Solvation energies of representative conformations of HuAtp12p during the final 20 ns of MD simulation

Conf. means conformation.

	Wild-type			W94R		
	Conf. 1	Conf. 2	Conf. 3	Conf. 1	Conf. 2	Conf. 3
Relative weight in ensemble	239	177	1	401	14	2
Polar contribution	−1185.2	−1043.1	−1086.0	−866.8	−949.7	−934.5
Apolar contribution	1081.4	1084.2	1078.9	1102.1	1098.0	1098.1
Total	−103.8	41.1	−7.1	235.3	148.3	163.6
Weighted Total	−59.49	17.44	−0.02	226.27	4.98	0.785
Weighted average		−42.06			232.03	

chondrial encephalomyopathy in a 14-month-old patient (16). Electron micrographs of the fibroblasts from the patient could not be distinguished from control cells on the basis of mitochondrial ultrastructure (Fig. 1), which is interesting in comparison to what Lefebve-Legendre *et al.* (46) reported from their work with Atp12p-deficient yeast cells. In the latter case, megadalton aggregates of unassembled F_1 α and β subunits accumulate inside mitochondria and are detected in electron micrographs of whole yeast cells as massive inclusion bodies that permeate the matrix obliterating normal cristae structure (46). The absence of similar electron-dense elements in the sample from the patient might reflect a positive selection over time in the fibroblast cultures for cells with normal mitochondrial morphology or indicate a significant difference in the response of human fibroblasts to an F_1 assembly defect *versus* what is observed in yeast *atp12* mutants. As samples become available in the future from new patients diagnosed with HuAtp12p deficiency, it will be of interest to determine whether mitochondria from freshly prepared cells show evidence of an unassembled F_1 protein storage defect and to compare the results obtained with fibroblasts *versus* more metabolically active tissues.

We took advantage of the facts that first the respiratory defect of Δatp12 yeast is rescued by providing wild type HuAtp12p on a plasmid (17), and second, the human protein is detected in mitochondria with polyclonal antibodies raised against ScAtp12p (Fig. 3*C*) to determine the consequences of the W94R mutation *in vivo*. A Δatp12 transformant harboring a multicopy plasmid for HuAtp12p(W94R) failed to grow on nonfermentable carbons (EG media), and mitochondria isolated from this strain were completely deficient in oligomycin-sensitive ATPase activity (Table 3). In the absence of a high resolution structure for Atp12p at the time this study was initiated, we took a "blind" approach to site-directed mutagenesis of Trp-94 and probed the consequences of replacing this amino acid with a different positively charged residue (W94K) or with one that was negatively charged (W94E), nonpolar bulky (W94F), or nonpolar nonbulky (W94A). The results of transforming Δatp12 with individual plasmids showed that the W94F protein rescued the respiratory deficiency of the yeast strain, whereas the Lys, Glu, and Ala substitutions all phenocopied the W94R mutation and gave rise to EG− yeast that lacked oligomycin-sensitive mitochondrial ATPase (Table 3). Western blots detected wild type and W94F HuAtp12p in soluble mitochondrial extracts, as opposed to the Arg, Ala, Glu, and Lys mutant proteins, which were absent from this fraction (Fig. 3, *B* and *C*, *S lanes*). With respect to the latter four samples, the 36–38-kDa immunoreactive proteins detected in whole mitochondria are probably the plasmid-borne HuAtp12p variants in most, if not all, cases. However, the putative mutant proteins were shown to be completely insoluble (Fig. 3, *B* and *C*, *P lanes*). Abnormal physical properties were observed also in experiments designed to overproduce and purify HuAtp12p(W94R) from bacterial hosts (Fig. 2). Cumulatively, these results provide evidence that a nonconservative substitution of Trp-94 in HuAtp12p has a substantial negative impact on the protein structure in the aqueous environment. A rationalization of the alteration of the physical properties of HuAtp12p responsible for these findings was provided by extensive MD simulation in solution of the wild type and mutant protein. Altogether, we carried out 80 ns of MD dynamics with all-atom models of the two proteins; the mutant protein was found to be conformationally more "rigid" than the wild type, and the alterations of its equilibrium surface in solution (Fig. 8) were associated with significantly more positive solvation energies. This latter finding provides a direct physical explanation for the reduced solubility of the W94R protein observed experimentally.

Unexpected findings from studies in which Δatp12 was transformed to produce *S. cerevisiae* Atp12p with the homologous "W94R" mutation (W103R in the case of ScAtp12p) ultimately led to the discovery that the physical defect imposed by the mutation can be rescued by another protein. Plasmid-encoded ScAtp12p(W103R) rescues the respiratory deficiency of Δatp12 in an otherwise wild type genetic background, but this capacity is lost when the gene for Fmc1p is co-deleted from the yeast nuclear genome. Lefebvre-Legendre *et al.* (21) had shown

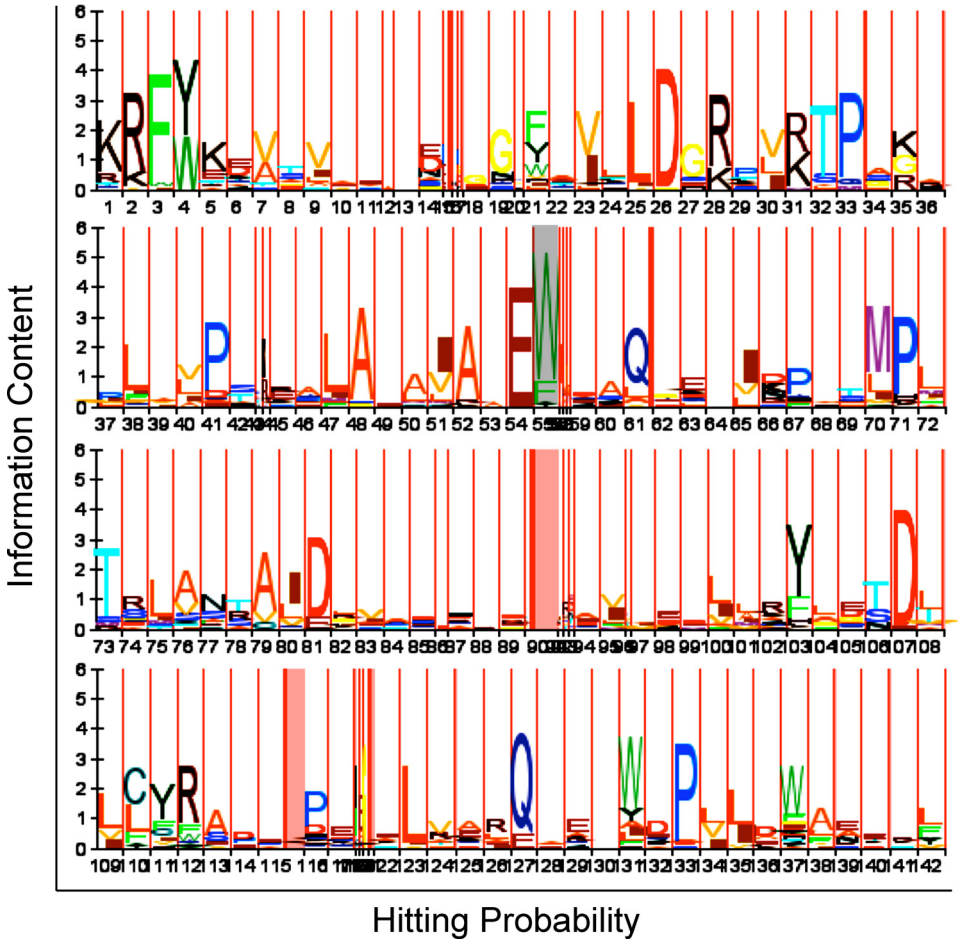

FIGURE 9. **HMM Logo for Atp12p.** The HMM logo for the Atp12p Pfam domain consists of alternating stacks for match (*white*) and insert (*red*) states for all positions in the sequence. The stack height (*information content*) indicates the sequence conservation at that position, whereas the *height* of the letters within the stack indicate the relative frequency of each amino acid at that position. The *stack width* (*hitting probability*) indicates the frequency of having an amino acid at that position; narrow *white stacks* denote high probability of amino acid deletion, and wide *red stacks* denote high probability of amino acid insertion. The stack corresponding to Trp-94 of HuAtp12p is annotated with *gray shading*.

previously that the loss of Fmc1p produces a conditional respiratory defect in yeast (cells grow on nonfermentable carbons at 30 °C and die at 37 °C), that this phenotype is rescued by supplying at least one extra copy of *ATP12* on a plasmid, and that Atp12p was reduced to nearly undetectable levels in mitochondria from Δfmc1 yeast cultured at 37 °C (21). The prediction that Fmc1p is necessary for ScAtp12p *in vivo* (21) is supported by our observation that the amount of Atp12p is significantly reduced in mitochondria isolated from a Δfmc1 strain grown at the permissive temperature (data not shown). The observations that pSc12p(W103R)^{CEN} just barely rescued the respiratory deficiency of Δatp12Δfmc1 at 30 °C (Fig. 4) and did not restore mitochondrial ATPase activity to the double mutant, and that pSc12p(W103R)$^{2\mu}$ failed completely to suppress the temperature-sensitive phenotype of Δfmc1 incubated at 37 °C suggest that the mutation affects an aspect of ScAtp12p that is under the control of Fmc1p. A search of the protein data base with the Fmc1p primary sequence suggests that the protein may be limited to fungi. Consistent with this idea, efforts to complement the temperature-sensitive phenotype of Δfmc1 with a human cDNA library carried in a yeast plasmid yielded no positive clones among 5 × 10^6 transformants.[4] However, the demonstration that Fmc1p promotes the activity of ScAtp12p(W103R), which is by itself nonfunctional, provides a proof of concept to support the discovery of agents that may modulate the action of HuAtp12p in human mitochondria.

Computational analysis of the amino acid sequences of Atp12p protein family members (Pfam 07542) further indicates the relevance of human Trp-94 in the context of Atp12p domain structure. Family groupings in the Pfam data base are based on Profile Hidden Markov Models (pHMM), which are probabilistic descriptions of emissions and transitions in a temporal pattern (*e.g.* amino acid sequence) (51). A Pfam HMM profile specifies a probability distribution over the 20 common amino acids for a match, a deletion, or an insertion at each position in the sequence, taking into consideration the background frequency for each amino acid. This information is visualized for Atp12p using an HMM logo (Fig. 9) (52). The Atp12p Pfam sequence spans the entire N-terminal domain and the first third of the C-terminal domain of the protein. The relevant tryptophan is indicated by the *gray-shaded rectangle* in Fig. 9 in the HMM logo for Atp12p. The height of the emission profile for the position corresponding to this tryptophan indicates that this is the most highly conserved position in the logo. Moreover, the letter sizing indicates that this position is most frequently populated by tryptophan, followed by phenylalanine. Thus, the W94R mutation in HuAtp12p that was isolated clinically alters the protein at a position in the sequence deemed critical during evolution.

REFERENCES

1. Boyer, P. D. (1997) *Annu. Rev. Biochem.* **66,** 717–749
2. Ackerman, S. H., and Tzagoloff, A. (2005) *Prog. Nucleic Acids Res. Mol. Biol.* **80,** 95–133
3. Senior, A. E., Nadanaciva, S., and Weber, J. (2002) *Biochim. Biophys. Acta* **1553,** 188–211
4. Bianchet, M. A., Hullihen, J., Pedersen, P. L., and Amzel, L. M. (1998) *Proc. Natl. Acad. Sci. U.S.A.* **95,** 11065–11070
5. Abrahams, J. P., Leslie, A. G., Lutter, R., and Walker, J. E. (1994) *Nature* **370,** 621–628
6. Kabaleeswaran, V., Puri, N., Walker, J. E., Leslie, A. G., and Mueller, D. M.

[4] J. P. di Rago, unpublished studies.

(2006) *EMBO J.* **25,** 5433–5442
7. Chinnery, P. F., and Schon, E. A. (2003) *J. Neurol. Neurosurg. Psychiatry* **74,** 1188–1199
8. Santamaria, M., Lanave, C., Vicario, S., and Saccone, C. (2007) *Biol. Chem.* **388,** 943–946
9. Wallace, D. C. (2005) *Annu. Rev. Genet.* **39,** 359–407
10. Santorelli, F. M., Shanske, S., Macaya, A., DeVivo, D. C., and DiMauro, S. (1993) *Ann. Neurol.* **34,** 827–834
11. Pastores, G. M., Santorelli, F. M., Shanske, S., Gelb, B. D., Fyfe, B., Wolfe, D., and Willner, J. P. (1994) *Am. J. Med. Genet.* **50,** 265–271
12. Debray, F. G., Lambert, M., Lortie, A., Vanasse, M., and Mitchell, G. A. (2007) *Am. J. Med. Genet. A* **143,** 2046–2051
13. Jonckheere, A. I., Hogeveen, M., Nijtmans, L. G., van den Brand, M. A., Janssen, A. J., Diepstra, J. H., van den Brandt, F. C., van den Heuvel, L. P., Hol, F. A., Hofste, T. G., Kapusta, L., Dillmann, U., Shamdeen, M. G., Smeitink, J. A., and Rodenburg, R. J. (2008) *J. Med. Genet.* **45,** 129–133
14. Sperl, W., Jesina, P., Zeman, J., Mayr, J. A., Demeirleir, L., VanCoster, R., Pícková, A., Hansíková, H., Houst'ková, H., Krejcík, Z., Koch, J., Smet, J., Muss, W., Holme, E., and Houstek, J. (2006) *Neuromuscul. Disord.* **16,** 821–829
15. Cízková, A., Stránecký, V., Mayr, J. A., Tesarová, M., Havlícková, V., Paul, J., Ivánek, R., Kuss, A. W., Hansíková, H., Kaplanová, V., Vrbacký, M., Hartmannová, H., Nosková, L., Honzík, T., Drahota, Z., Magner, M., Hejzlarová, K., Sperl, W., Zeman, J., Houstek, J., and Kmoch, S. (2008) *Nat. Genet.* **40,** 1288–1290
16. De Meirleir, L., Seneca, S., Lissens, W., De Clercq, I., Eyskens, F., Gerlo, E., Smet, J., and Van Coster, R. (2004) *J. Med. Genet.* **41,** 120–124
17. Wang, Z. G., White, P. S., and Ackerman, S. H. (2001) *J. Biol. Chem.* **276,** 30773–30778
18. Wang, Z. G., Sheluho, D., Gatti, D. L., and Ackerman, S. H. (2000) *EMBO J.* **19,** 1486–1493
19. Ackerman, S. H., and Tzagoloff, A. (1990) *Proc. Natl. Acad. Sci. U.S.A.* **87,** 4986–4990
20. Hinton, A., Gatti, D. L., and Ackerman, S. H. (2004) *J. Biol. Chem.* **279,** 9016–9022
21. Lefebvre-Legendre, L., Vaillier, J., Benabdelhak, H., Velours, J., Slonimski, P. P., and di Rago, J. P. (2001) *J. Biol. Chem.* **276,** 6789–6796
22. Bowman, S., Ackerman, S. H., Griffiths, D. E., and Tzagoloff, A. (1991) *J. Biol. Chem.* **266,** 7517–7523
23. Hill, J. E., Myers, A. M., Koerner, T. J., and Tzagoloff, A. (1986) *Yeast* **2,** 163–167
24. Ludlam, A., Brunzelle, J., Pribyl, T., Xu, X., Gatti, D. L., and Ackerman, S. H. (2009) *J. Biol. Chem.* **284,** 17138–17146
25. Berendsen, H. J., Postma, J. P., van Gunsteren, W. F., and Hermans, J. (1981) in *Intermolecular Forces* (Pullman, B., ed), Reidel Publishing Co., Dordrecht, Netherlands
26. Bowers, K. J., Chow, E., Xu, H., Dror, R. O., Eastwood, M. P., Gregerson, B. A., Klepeis, J. L., Kolossvary, I., Moraes, M. A., Sacerdoti, F. D., Salmon, J. K., Shan, Y., and Shaw, D. E. (2006) *Proceedings of the 2006 ACM/IEEE Conference on Supercomputing (SC06), November 11–17, 2006*, p. 43, IEEE Computer Society, Tampa, FL
27. Nocedal, J. (1980) *Mathematics of Computation* **35,** 773–782
28. Byrd, R. H., Nocedal, J., and Schnabel, R. B. (1994) *Mathematical Programming* **63,** 129–156
29. Jorgensen, W. L., Maxwell, D. S., and Tirado-Rives, J. (1996) *J. Am. Chem. Soc.* **118,** 11225–11236
30. Essmann, U., Perera, L., Berkowitz, M. L., Darden, T., Lee, H., and Pedersen, L. G. (1995) *J. Chem. Phys.* **103,** 8577–8593
31. Evans, D. J., and Holian, B. L. (1985) *J. Chem. Phys.* **83,** 4069–4074
32. Martyna, G. J., Tobias, D. J., and Klein, M. L. (1994) *J. Chem. Phys.* **101,** 4177–4189
33. Tuckerman, M., Berne, B. J., and Martyna, G. J. (1992) *J. Chem. Phys.* **97,** 1990–2001
34. Ryckaert, J. P., Ciccotti, G., and Berendsen, H. J. (1977) *J. Comput. Phys.* **23,** 327–341
35. Baker, N. A., Sept, D., Joseph, S., Holst, M. J., and McCammon, J. A. (2001) *Proc. Natl. Acad. Sci. U.S.A.* **98,** 10037–10041
36. Warshel, A., Sharma, P. K., Kato, M., and Parson, W. W. (2006) *Biochim. Biophys. Acta* **1764,** 1647–1676
37. Schutz, C. N., and Warshel, A. (2001) *Proteins Struct. Funct. Genet.* **44,** 400–417
38. Sept, D., Elcock, A. H., and McCammon, J. A. (1999) *J. Mol. Biol.* **294,** 1181–1189
39. Ponder, J. W., and Case, D. A. (2003) *Adv. Protein Chem.* **66,** 27–85
40. Metoki, K., and Hommes, F. A. (1984) *J. Inherited Metab. Dis.* **7,** 9–11
41. Li, H., Robertson, A. D., and Jensen, J. H. (2005) *Proteins* **61,** 704–721
42. Wagoner, J. A., and Baker, N. A. (2006) *Proc. Natl. Acad. Sci. U.S.A.* **103,** 8331–8336
43. DeLano, W. L. (2007) *The PyMOL Molecular Graphics System,* DeLano Scientific LLC, Palo Alto, CA
44. Schiestl, R. H., and Gietz, R. D. (1989) *Curr. Genet.* **16,** 339–346
45. Lowry, O. H., Rosebrough, N. J., Farr, A. L., and Randall, R. J. (1951) *J. Biol. Chem.* **193,** 265–275
46. Lefebvre-Legendre, L., Salin, B., Schaëffer, J., Brèthes, D., Dautant, A., Ackerman, S. H., and di Rago, J. P. (2005) *J. Biol. Chem.* **280,** 18386–18392
47. Basu, T., and Poddar, R. K. (1997) *Biochem. Mol. Biol. Int.* **41,** 1093–1100
48. Mukhopadhyay, A., Uh, M., and Mueller, D. M. (1994) *FEBS Lett.* **343,** 160–164
49. Wang, Z. G., and Ackerman, S. H. (1998) *J. Biol. Chem.* **273,** 2993–3002
50. Ackerman, S. H. (2002) *Biochim. Biophys. Acta* **1555,** 101–105
51. Eddy, S. R. (1998) *Bioinformatics* **14,** 755–763
52. Schuster-Böckler, B., Schultz, J., and Rahmann, S. (2004) *BMC Bioinformatics* **5,** 7
53. Ackerman, S. H., and Tzagoloff, A. (2007) *Methods Mol. Biol.* **372,** 363–377